Universiteit
Leiden
The Netherlands

Transdermal iontophoresis of dopaminergic (pro) drugs : from formulation to in vivo application

Ackaert, O.

Citation
Ackaert, O. (2010, April 28). *Transdermal iontophoresis of dopaminergic (pro) drugs : from formulation to in vivo application*. Retrieved from https://hdl.handle.net/1887/15336

Version:	Corrected Publisher's Version
License:	Licence agreement concerning inclusion of doctoral thesis in the Institutional Repository of the University of Leiden
Downloaded from:	https://hdl.handle.net/1887/15336

Note: To cite this publication please use the final published version (if applicable).

5

Transdermal iontophoretic delivery of a novel series of dopamine agonists *in vitro*: physicochemical considerations

Oliver W. Ackaert[a], Jeroen De Graan[c], Romano Capancioni[a], Durk Dijkstra[c], Meindert Danhof[b] and Joke A. Bouwstra[a]

[a]Division of Drug Delivery Technology, Leiden/Amsterdam Center for Drug Research, Leiden, The Netherlands

[b]Division of Pharmacology, Leiden/Amsterdam Center for Drug Research, Leiden, The Netherlands

[c]Department of Medicinal Chemistry, University Center of Pharmacy, University of Groningen, Groningen, The Netherlands

adapted from *Journal of pharmacy and pharmacology*. 2010. *in press*

Abstract

The transdermal iontophoretic delivery of a novel series of 2-aminotetraline and chromanamine based dopamine agonists was investigated *in vitro*. Systematic structural modifications allowed us to investigate their effect on solubility in the donor phase and iontophoretic delivery across human skin. Transport profiles were analyzed with nonlinear mixed effect modeling, utilizing an extension to an existing compartmental model. Furthermore relationships between physicochemical properties and transport parameters were addressed. A solubility increase was observed: 5,6-di-OH-DPAT < 5-OH-MPAT < 5-OH-EPAT < 8-OH-DPAC. The structure significantly affected the iontophoretic delivery across human stratum corneum and dermatomed human skin with the highest flux for 5-OH-EPAT and 5-OH-MPAT. The extended model with two skin release constants (K_{R1}, K_{R2}) describes more adequately iontophoretic transport profiles than the existing model with one release constant. The extended model suggests 2 parallel transport pathways during current application. Across human stratum corneum the electrophoretic mobility, measured with capillary electrophoresis, showed a linear relationship with the electromigrative flux and the zero order iontophoretic mass input into the skin (I_0). Combining transport parameters (I_0, K_{R1} and K_{R2}), predicted from physicochemical properties, with compartmental modeling provides a powerful tool to simulate iontophoretic transport profiles for screening potential candidates and designing experiments.

Keywords: transdermal, iontophoresis, dopamine agonists, modeling, transport pathway

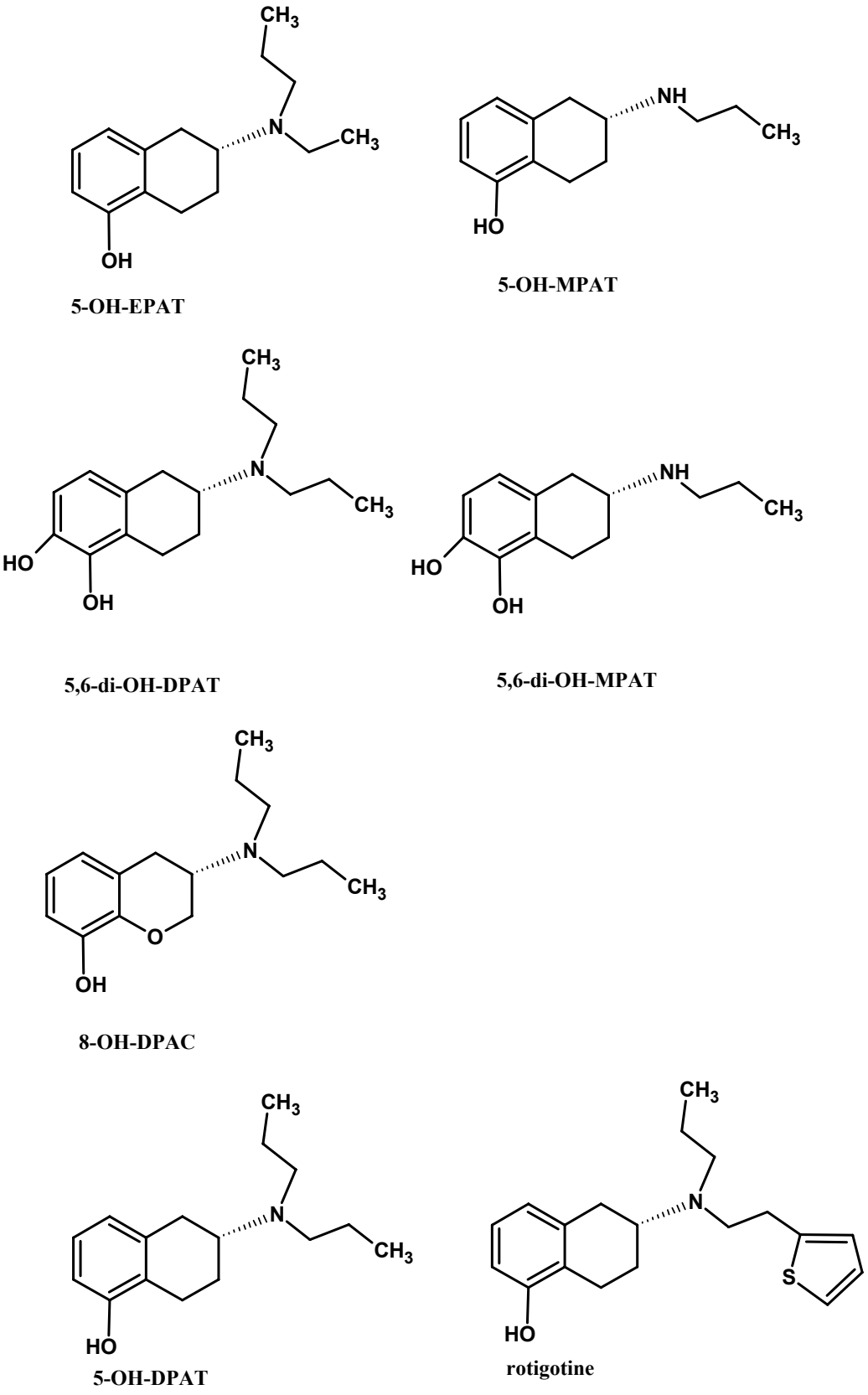

Figure 1: The chemical structures of different dopamine agonists

1 Introduction

Transdermal iontophoresis enhances the delivery of small charged solutes across the skin by application of a small current (≤0.5 $mA.cm^{-2}$) across this membrane. Important advantages of transdermal delivery are circumvention of the hepatic first-pass effect and a continuous administration of the drug. A particular advantage of iontophoresis is the possibility to adjust the rate of delivery by changing the current density [1]. For the symptomatic treatment of Parkinson's disease (Pd) the current strategy is to administer therapeutic agents in a continuous manner to reduce the induction of motor fluctuations after long term use [2-4]. Most of the dopamine agonists have a very narrow therapeutic window, which demands for an accurate individualized titration, adjusted to the needs of the therapy [5-6]. For these reasons, the *in vitro* and *in vivo* iontophoretic delivery of dopamine agonists, such as apomorphine, ropinorole, 5-OH-DPAT and rotigotine, have been intensively investigated [7-16].

To improve the transport efficiency and consequently the therapeutic treatment of Pd, a good understanding is required about the structure-transport relationship. However, with respect to this class of drugs little is known about the structure-transport relationship. In the present study the *in vitro* iontophoretic delivery is investigated of a new series of dopamine agonists, which were selected based on their potency and their molecular structure [17-23]. The small structural differences allow us to investigate in detail the influence of molecular structure and related physicochemical properties of the dopamine agonists on the iontophoretic transport efficiency.

During the years several studies have focused on selecting the key physicochemical properties that determine the transdermal iontophoretic delivery efficiency. It has been reported that the size of the solute, expressed as molecular weight (Mw) or molecular volume (MV), is an important descriptor with a higher transport for smaller molecules [24-26]. Furthermore, an increase in charge/Mw ratio results in an increase in transdermal electromigrative flux, as was observed for a series of peptides [27]. In a follow up study by Abla *et al*. the electrophoretic mobility, measured by capillary zone electrophoresis (CZE), provided an estimation of the electromigrative flux [28]. Finally, the lipophilicity of the transported molecules also affects the transdermal iontophoretic transport, however the relationship with the corresponding transport efficiency is not so straightforward as with passive diffusion [29-30].

Most of these physicochemical property-transport relationships use a single parameter to describe the transdermal iontophoretic flux. As a single end-point the flux at the end of the iontophoresis period or the steady state flux and lag time are often selected. However in these approaches, the information on the shape of the iontophoresis transport curve is neglected, which makes extrapolation towards the *in vivo* situation more difficult. The mathematical models, introduced by Nugroho *et al*., were designed to overcome the aforementioned disadvantages and to make the extrapolation from the *in vitro* to *in vivo* transport studies more reliable [16, 31-32]. The proposed models were based on a commonly used assumption for iontophoresis, namely a constant mass input into the skin during iontophoresis due to the constant iontophoretic driving force resulting from the application of a constant current. An adapted model, based on the compartmental models introduced by Nugroho *et al*. [16, 31], is presented and applied to describe the iontophoretic flux profile of this series of dopamine agonists. In this study the relationship between the physicochemical properties and the transport is addressed, using the electromigrative flux as single end-point and using the adapted model describing the total iontophoretic flux profile.

The objectives of the present work are: (i) to investigate the transdermal iontophoretic delivery *in vitro* of a new series of dopamine agonists, (ii) to evaluate the adapted mathematical compartmental model to describe the *in vitro* iontophoretic delivery of these dopamine agonists and (iii) to study the relationship(s) between the physicochemical properties (clogP, electrophoretic mobility and molecular weight) of the molecules and the J_{EM} and the parameter estimates (zero order mass input from donor to skin and skin release constants), using the adapted model.

2 Materials and methods

The 2-aminotetralines 5-Hydroxy-2-(N-ethyl,N-n-propylamino)tetralin (5-OH-EPAT.HBr), 5-Hydroxy-2-(N-n-propylamino)tetralin (5-OH-MPAT.HBr), 5,6-di-hydroxy-2-(N-n-propylamino)tetralin (5,6-di-OH-MPAT.HBr), 5,6-di-hydroxy-2-(N,N-di-n-propylamino)tetralin (5,6-di-OH-DPAT.HBr), 5-hydroxy-2-(N,N,-di-n-propylamino)tetralin (5-OH-DPAT.HBr) and the chromanamine 8-hydroxy-3-(N,N,-di-n-propylamino)chroman (8-OH-DPAC.HBr) (Figure 1; purity > 95%, determined with HPLC and NMR) were synthesized at the Department of Medicinal Chemistry of the University of Groningen, Groningen, the Netherlands. Silver, silver chloride (purity >99.99%), Trypsin (Type III from bovine pancreas) and trypsin inhibitor (Type II-S from soybean) were obtained from Sigma-Aldrich (Zwijndrecht, The

Netherlands). Acetaminophen was purchased from Brocacef BV (Maarssen, the Netherlands) and D-Mannitol was obtained from BDH Laboratory supplies (Poole, UK). Spectra/Por® RC dialysis membrane disks (cut off value of 6000-8000 Da) were purchased from Spectrum laboratories, Inc (Rancho Dominquez, Ca, USA). Tetrahydrofuran (THF, stabilized, purity > 99.8%) was obtained from Biosolve (Valkenswaard, the Netherlands). Triethylamine (TEA, purity > 99%) was obtained from Acros Organics (Geel, Belgium). All other chemicals and solvents were of analytical grade. All solutions were prepared in Millipore water with a resistance of more than 18 MΩ.cm.

2.1 Maximum solubility

The solubility studies of the different compounds were carried out as described elsewhere [14]. Briefly, each compound was solubilized in citric buffer 5 mM, pH 5.0 + 4 $g.l^{-1}$ NaCl + 23.1 $g.l^{-1}$ D-mannitol. Subsequently the pH in each test tube was adjusted to pH 5.0 with 1M NaOH or 1M HCl under continuous shaking. Each solution was shaken for 48h, after which the solution was centrifuged and filtered. The concentration in each solution was determined with HPLC.

2.2 Stability of 5,6-di-OH-MPAT and 5,6-di-OH-DPAT

The oxidation of 5,6-di-OH-MPAT and 5,6-di-OH-DPAT was investigated under various conditions. At the starting point 0.1 $mg.ml^{-1}$ of 5,6-di-OH-DPAT and 5,6-di-OH-MPAT were dissolved in the buffer solution. The solutions were continuously stirred and kept constant at the desired temperature, using a thermostat controlled water bath. If required a circular sheet of HSC (ø=18 mm) was added to the solution and a current of 320 μA was applied. At regular time intervals samples were taken from the solution and diluted in Millipore water, containing 2.86% v/v anti-oxidant solution (0.5% w/v ascorbic acid 0.05% w/v EDTA and 25% v/v H_3PO_4) to prevent the molecule to further oxidize. The amount of remaining drug was quantified by RP-HPLC (section 2.6).

2.3 Capillary electrophoresis

Previous studies have shown that the electrophoretic mobility at pH 7.4 is related to the iontophoretic mobility during transdermal transport [28, 33]. The electrophoretic mobility of various compounds in the current study was investigated with capillary electrophoresis (CE). These experiments were performed using a HPCE system (modelnumber: G1600OAX, Agilent Technologies, Amstelveen, The Netherlands) equipped with an on-column diode-array detector, an autosampler, and a 30 kV

power supply. CE Chemstation (Agilent Technologies) was used for CE control, data acquisition, and handling. The separation was performed in a 50 µm fused-silica capillary 48.5 cm in total length, and 40 cm to the UV detector. All experiments were carried out in cationic mode (the anode at the inlet and cathode at the outlet). The concentration of the samples was 0.5 mM in water and DMSO in water (0.5% v/v) was added to the solution as a marker for the electroosmotic flow. The electrophoretic mobility was determined using a phosphate buffer pH 7.4 (Na_2HPO_4: 5.82 $g.l^{-1}$; NaH_2PO_4: 5.1 $g.l^{-1}$) as electrolyte solution (mobile phase). UV detection was applied at 220 and 278 nm for the detection of DMSO and the molecule, respectively. The capillary was preconditioned as follows: 5 min 0.1 M NaOH + 10 min electrolyte solution. The sample was injected during 5 sec under a pressure of 50 mbar. Every sample was measured 3 times and every analysis a fresh electrolyte solution was used. The effective electrophoretic mobility (μ_{eff}) was calculated as follows:

$$\mu_{eff} = \mu_{obs} - \mu_{EOF} = \frac{L_{tot} L_{eff}}{V} \left[\left(\frac{1}{t_{obs}}\right) - \left(\frac{1}{t_{EOF}}\right) \right] \quad (1)$$

with μ_{obs} and μ_{EOF} as the electrophoretic mobility of the compound and the electroosmotic marker DMSO, respectively. Furthermore L_{tot} and L_{eff} are the total distance of the capillary and the distance from the inlet to the detection point, respectively. t_{obs} and t_{EOF} are the time required to reach the detection point for the analyte and the electroosmotic marker DMSO, respectively and V is the applied voltage [34-35].

2.4 *In vitro* transport studies

The preparation of dermatomed human skin (DHS) and human stratum corneum (HSC) was performed according to the method described previously [15]. All transport experiments were carried out as described elsewhere [15]. The donor formulation (citric buffer 5 mM, pH 5.0, NaCl: 4 $g.l^{-1}$, D-mannitol: 23.1 $g.l^{-1}$), containing the solute, was added to the anodal chamber. The cathodal chamber was filled with PBS pH 7.4 (NaCl: 8 $g.l^{-1}$, Na_2HPO_4: 2.86 $g.l^{-1}$, KH_2PO_4: 0.2 $g.l^{-1}$, KCl: 0.19 $g.l^{-1}$). The acceptor phase, maintained at 32°C, was continuously perfused with PBS pH 7.4 at a flow rate of 7.0 $ml.h^{-1}$. The following protocol was used: 6h passive diffusion + 9h iontophoresis (500 $\mu A.cm^{-2}$) + 5h passive diffusion. Samples were collected every hour with an automatic fraction collector (ISCO Retriever IV, Beun De Ronde BV, Abcoude, The Netherlands). The specific conditions of the individual transport studies are described below. To prevent oxidation of 5,6-di-OH-DPAT and 5,6-di-OH-MPAT after transdermal transport and prior to analysis, 200 µl of the anti-

oxidant solution (EDTA (Titriplex III): 0.5 $g.l^{-1}$, $Na_2S_2O_5$: 5 $g.l^{-1}$, H_3PO_4 (85 wt. % in H_2O): 294 $ml.l^{-1}$) was added to every collecting tube in the fraction collector.

2.4.1 Total iontophoretic flux

The iontophoretic delivery of 5-OH-EPAT, 5-OH-MPAT, 5,6-di-OH-MPAT and 5,6-di-OH-DPAT and 8-OH-DPAC across HSC was studied at 3.9 mM. Two additional concentrations (1.5 and 7.0 mM) of 5-OH-EPAT and 5-OH-MPAT were studied. Of 5-OH-EPAT, 5-OH-MPAT, 5,6-di-OH-DPAT, 5-OH-DPAT and 8-OH-DPAC, transport studies across DHS were performed using a donor concentration of 3.9 mM.

2.4.2 Electroosmotic flux

According to the Nernst-planck Equation the total flux (J_{tot}) consists of three transport mechanisms:

$$J_{tot} = J_{EM} + J_{EO} + J_P \qquad (2)$$

with the electromigrative flux (J_{EM}) and the electroosmotic flux (J_{EO}) as the principal driving mechanisms for iontophoresis of charged species. The passive flux (J_P) is often negligible. The electroosmotic flux across HSC was investigated during iontophoretic transport of 5-OH-EPAT, 5-OH-MPAT, 5,6-di-OH-DPAT and 8-OH-DPAC (3.9 mM). Acetaminophen (15 mM) was added to the donor phase as a marker for the electroosmotic flux. The electroosmotic flux was calculated, using the following Equation, assuming a similar electroosmotic transport for the analogs and acetaminophen:

$$J_{EO} = \frac{J_{ace}}{C_{ace}} x C_m \qquad (3)$$

with J_{ace} as the flux of acetaminophen and C_m and C_{ace} as the donor concentration of the molecule and acetaminophen, respectively.

2.5 Compartmental modelling

The iontophoretic transport *in vitro* of different molecules was analyzed using non-linear mixed effects modelling. The starting point of the models is a zero order mass transport form the donor solution into the skin during and after iontophoresis. In this paper an extension to the basic model is presented.

2.5.1 Basic model *in vitro*

An extensive explanation and description of the basic model is presented elsewhere [31]. Briefly, the basic model assumes a constant rate of mass input from the donor into the skin during iontophoresis due to a constant iontophoretic driving force. Based on this assumption the equations, to describe *in vitro* iontophoretic transport during (Equation 4) and after current application (Equation 6) are:

$$J(t) = \frac{I_0}{S}(1 - e^{-K_R.(t-t_L)}) \tag{4}$$

$$J_{ss} = \frac{I_0}{S} \tag{5}$$

$$J(t) = \frac{P_{PI}}{S}(1 - e^{-K_R.(t-T)}) + \frac{I_0}{S}(1 - e^{-K_R.(T-t_L)}).e^{-K_R(t-T)} \tag{6}$$

where $J(t)$ is the flux at time t and S is the diffusion area, K_R is a first order skin release rate constant, I_0 the zero-order iontophoretic mass transfer from the donor compartment into the skin compartment during current application, t_L is the kinetic lag time parameter, introduced to address the time required for drug molecules to enter the skin compartment, T is time of current application, J_{ss} is the flux at steady state and P_{PI} is the zero order drug input due to the passive driving force post-iontophoresis.

2.5.2 Extended model *in vitro*

As observed from the iontophoretic flux profile of the compounds presented in this paper, the flux increases in time during the current application. This suggests that two transport routes are involved in the iontophoretic delivery, linked in parallel. The observed flux is the total amount of drug released in the acceptor compartment. In analogy to the basic model the zero order mass transfer from the donor into the skin remains constant, but the first order release constant from the skin to the acceptor will be different for both transport mechanisms. Therefore the iontophoretic flux *in vitro* during iontophoresis ($t \leq T$) can be described by the equation:

$$J(t) = \frac{I_0}{S}(1 - e^{-K_{R1}.(t-t_L)}) + \frac{I_0}{S}(1 - e^{-K_{R2}.(t-t_L)}) \tag{7}$$

$$J_{ss} = 2 * \frac{I_0}{S} \tag{8}$$

With K_{R1} and K_{R2} as the release constants to describe both transport routes. During the post iontophoresis period (t>T) only one release constant appeared to be sufficient to describe the passive flux, resulting in the following Equation:

$$J(t) = \frac{P_{PI}}{S}(1 - e^{-K_{R2}.(t-T)}) + \left(\frac{I_0}{S}(1 - e^{-K_{R1}.(T-t_L)}) + \frac{I_0}{S}(1 - e^{-K_{R2}.(T-t_L)}) \right).e^{-K_{R2}(t-T)} \quad (9)$$

2.5.3 Curve fitting and model evaluation

Fitting the data was performed using the subroutines ADVANCE6 TRANS1 TOL=5 from PREDPP in NONMEM (NONMEM version VI). Interindividual variability was modeled using an exponential model and the residual error was characterized by an exponential and/or additive error model. The estimation of the population parameters was performed using a conventional first order method [36].
The extended model was evaluated in comparison to the basic model. The statistical analysis was based on the objective function, which is defined as -2 times the logarithm of the likelihood. If the objective function of the extended model with 2 release constants during the current application, decreases with a value of 3.84 (and/or more) compared to the objective function of the basic model, the extended model is significantly better ($p<0.05$; χ^2-test).

2.6 Analytical method

Different HPLC methods were developed to analyze the respective molecule and acetaminophen by RP-HPLC. The aminotetralins and the chromanamine were detected using a scanning fluorescence detector (Waters™ 474, Millipore, Milford, MA, USA) and acetaminophen was detected using a UV detector (Dual λ Absorbance Detector 2487, Waters, Milford, USA). The column, the composition of the mobile phase, the volume of injection and the respective excitation and emission wavelengths to analyze the different compounds are depicted in Table 1. The flow rate was set to 1.0 $ml.min^{-1}$. Calibration curves showed a linear response between 100 and 40000 $ng.ml^{-1}$ ($R^2>0.99$). The limit of detection (LOD) and limit of quantification (LOQ) for these HPLC methods can also be found in Table 1.

2.7 Data analysis

All data are presented as mean ± standard deviation (SD) or as mean ± standard error of the mean (SEM). When a statistical analysis was performed comparing only 2 groups, a Students t-test was used. When 3 or more groups were compared, a 1-way ANOVA statistical analysis was executed. Comparing the effect of two factors

Table 1: The HPLC method of the different compounds investigated in the current paper including column, mobile phase composition, volume of injection, excitation wavelength (λ_{ex}), emission wavelength (λ_{em}), limit of detection (LOD) and limit of quantification (LOQ)

Compound	**Column**	**Mobile phase**			**Fluorescence**			
		Composition	TEA	injection volume	λ_{ex}	λ_{em}	LOD	LOQ
		(% v/v)	(mM)	(µl)	(nm)	(nm)	($ng.ml^{-1}$)	($ng.ml^{-1}$)
5-OH-EPAT	Superspher RP-select B C8	Ace 50 mM/THF 95/5	30	20	275	302	21.0	35.0
5-OH-MPAT	Inertsil 5ODS-2	Ace 100 mM/ACN 90/10	15	50	280	310	8.2	12.3
5,6-di-OH-DPAT	Superspher RP-select B C8	Ace 50 mM/THF 97/3	15	200	276	305	61.4	115.9
5,6-di-OH-MPAT	Inertsil 5ODS-2	Ace 50 mM/THF 96/4	15	50	280	310	90.7	150.5
8-OH-DPAC	Superspher RP-select B C8	Ace 50 mM/THF 95/5	30	50	277	306	29.9	44.9

Acetaminophen: mobile phase, column, limit of detection and quantification are dependent on the compound co-analyzed;
UV-detection: λ=243 nm;
Ace: acetatebuffer pH 3.6

simultaneously was performed using 2-way ANOVA. If the overall p-value was less than 0.05, a Bonferonni post-test was applied to compare different groups. Statistical tests were performed by using GraphPad Prism version 5.00 for Windows (GraphPad Software, San Diego, CA, USA). For all statistical analysis a significance level of $p<0.05$ was used.

3 Results

3.1 Maximum solubility

The maximum solubility of the different compounds was determined in citric buffer 5 mM at pH 5.0 in the presence of 68 mM NaCl and D-mannitol as this is the composition of the donor solution, used for transport studies. The results of the solubility assay can be found in Table 2. The solubility data of rotigotine.HCl and 5-OH-DPAT, adapted from literature, were added to the table for comparison. An increase in solubility was observed ranking the molecules in the following order:

Table 2: The physicochemical properties of the various compounds investigated. The molecular weight (Mw) and the calculated logP (clogP) are presented together with the solubility in a citric buffer 5mM pH 5.0, containing 4 $g.l^{-1}$ NaCl and 23.1 $g.l^{-1}$ D-mannitol, and the electophoretic mobility, determined with capillary electrophoresis. The solubility of 5-OH-DPAT and rotigotine, obtained from literature, are added to the table for comparison.

Compound	**Mw** ($g.mol^{-1}$)	**clogP[c]**	**Solubility** (mM)	**Electrophoretic mobility (μ_{em})** 10^{-4} ($cm^2.s^{-1}.V^{-1}$) mean ± SD
5-OH-EPAT	233.36	3.71	111.7	1.84 ± 0.01
5-OH-MPAT	205.30	2.93	93.1	1.88 ± 0.00
5,6-di-OH-DPAT	263.38	3.74	44.2	1.56 ± 0.01
5,6-di-OH-MPAT	221.30	2.5	n.d	1.61 ± 0.01
8-OH-DPAC	249.36	3.4	282.5	1.64 ± 0.01
5-OH-DPAT	247.38	4.15	56.7[a]	1.76 ± 0.01
rotigotine	315.48	4.82	7.1[b]	1.49 ± 0.04

[a,b]: value adapted from literature [14, 40]
[c]: cLogP was calculated using alogsP [37-39]
n.d.: not determined

rotigotine < 5,6-di-OH-DPAT < 5-OH-DPAT < 5-OH-MPAT < 5-OH-EPAT < 8-OH-DPAC. Furthermore the relative hydrophilicity of the different analogs, expressed with the octanol-water partition coefficient, clogP, was calculated/computed using the ALOGPS 2.1 webservice [37-39]. The results are also provided in Table 2.

3.2 Stability of 5,6-di-OH-MPAT and 5,6-di-OH-DPAT

The catecholgroup of 5,6-di-OH-MPAT and 5,6-di-OH-DPAT is expected to be susceptible to photo-, auto- and chemical oxidation to ortho-semiquinone and subsequently to ortho-quinone, similar as apomorphine, another catecholamine [41]. Therefore the stability of these 2 molecules was investigated under various conditions, mimicking the different compartments during *in vitro* iontophoretic transport. Figure 2, evaluating the % remaining catechol after 24h and 48h, shows that 5,6-di-OH-MPAT remains stable at pH 5.0 at room temperature. Increasing only

the temperature had little influence on the stability: after 48h the remaining 5,6-di-OH-MPAT was 95.9 % and 87.7 ± 5.6 % at room temperature and 32 °C, respectively. Addition of HSC and application of a current decreased the remaining drug from 96.2 ± 3.1% to 90.2% after 24h. In analogy to other catecholamines, the pH of the solution had a strong influence on the stability of the 2 compounds [41-42]. At pH 5.0 5,6-di-OH-MPAT and 5,6-di-OH-DPAT were more stable than at pH 6.0. Increasing the pH to 7.4 resulted even in a more pronounced degradation of 5,6-di-OH-MPAT.

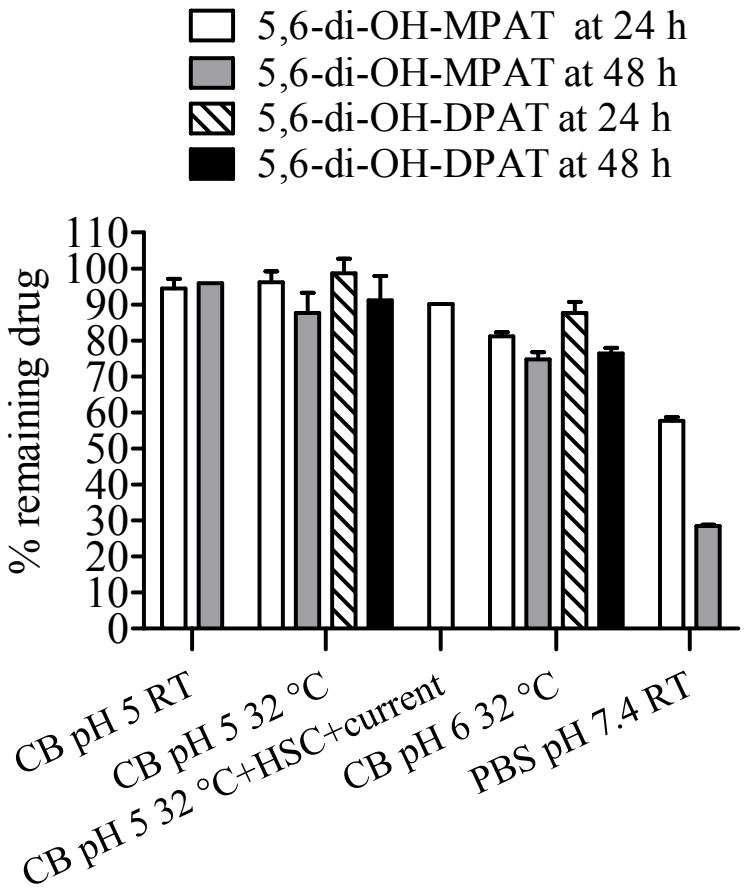

Figure 2: Bar plot of the % remaining 5,6-di-OH-MPAT after 24h (white) and 48h (grey) and of the % remaining 5,6-di-OH-DPAT after 24h (striped) and 48h (black) at various conditions. The data are presented as mean ± SD (n=2-3).
CB=citric buffer, Current=320µA, HSC=circular sheet of human stratum corneum (ø=18 mm), RT=room temperature.

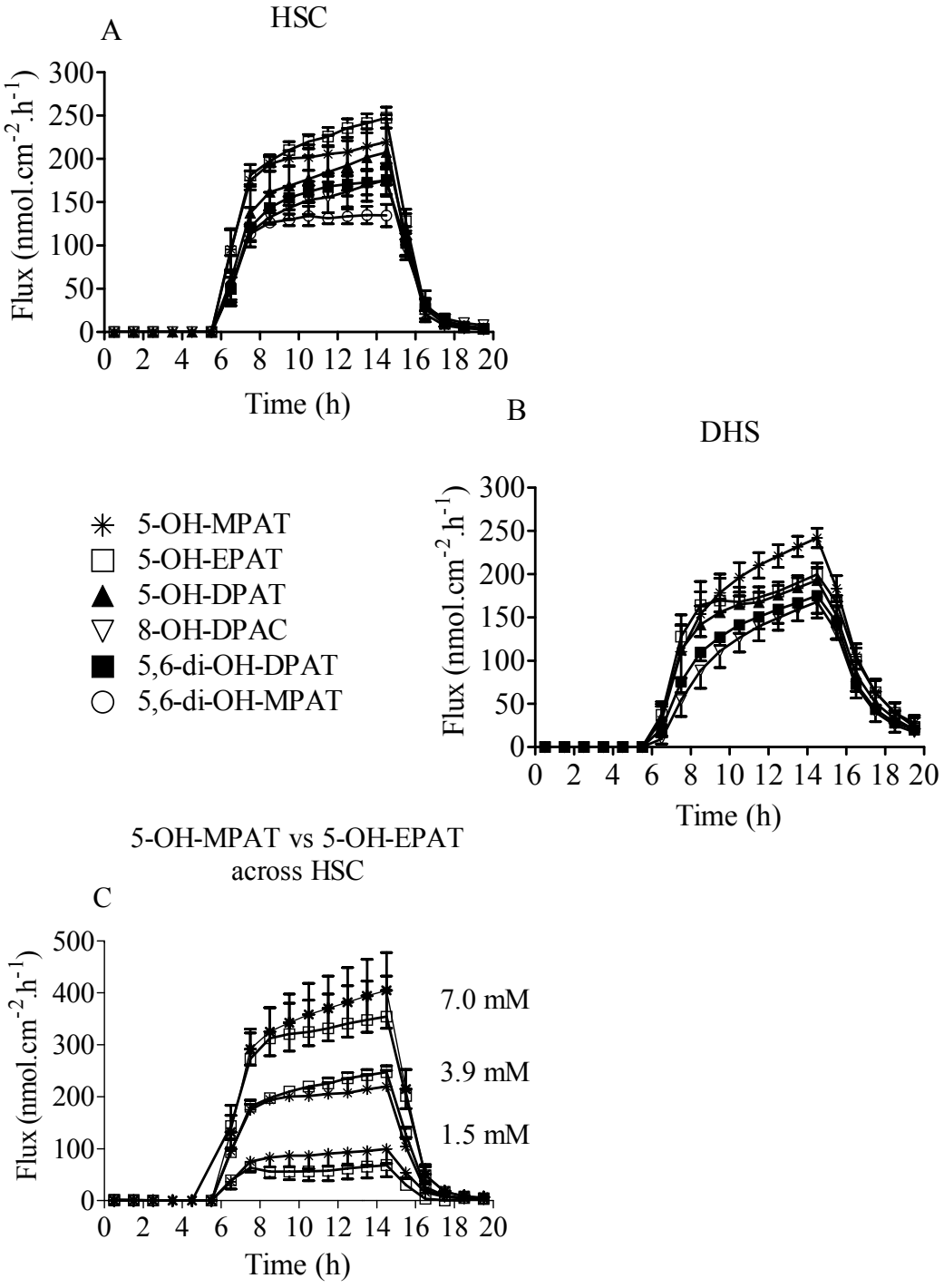

Figure 3: The iontophoretic flux profile of the different aminotetralines, 5-OH-MPAT (star), 5-OH-EPAT (open square), 5-OH-DPAT (closed triangle), 5,6-di-OH-DPAT (closed square), 5,6-di-OH-MPAT (open circle) and the chromanamine 8-OH-DPAC (open triangle) across two different skin types HSC (**A**) and across DHS (**B**). The donor concentration of all the compounds was 3.9 mM. Panel **C** shows the comparison of the iontophoretic flux vs time profile of 5-OH-MPAT (star) and 5-OH-EPAT (open square) across HCS at 3 different concentrations (1.5, 3.9, 7.0 mM). The data are presented as mean ± SD (n=4-7).

3.3 Capillary electrophoresis

To assess the electrophoretic mobility of the various compounds, capillary electrophoresis was performed. The results of the capillary electrophoresis are summarized in Table 2. The electrophoretic mobility of the various compounds increased in the following order: rotigotine 5,6-di-OH-DPAT < 5,6-di-OH-MPAT < 8-OH-DPAC < 5-OH-DPAT < 5-OH-EPAT < 5-OH-MPAT.

3.4 Iontophoretic transport

3.4.1 Total transport across HSC and DHS

Transport studies with the dopamine agonists at 3.9 mM were performed to compare the iontophoretic delivery of the various compounds. The different flux profiles of the analogs across HSC and DHS are depicted in Figure 3A and 3B, respectively. The flux of the different compounds was evaluated statistically after 9h of iontophoresis (current density is 500 $\mu A.cm^{-2}$). Across HSC 1-way ANOVA analysis showed an overall significant difference in the flux of the different compounds ($p<0.0001$). The observed flux after 9h increased in the following order: 5,6-di-OH-MPAT (134.5 ± 12.9 $nmol.cm^{-2}.h^{-1}$) < 5,6-di-OH-DPAT (175.0 ± 15.9 $nmol.cm^{-2}.h^{-1}$) < 8-OH-DPAC (175.9 ± 18.9 $nmol.cm^{-2}.h^{-1}$) < 5-OH-DPAT (207.7 ± 38.0 $nmol.cm^{-2}.h^{-1}$) < 5-OH-MPAT (219.7 ± 31.4 $nmol.cm^{-2}.h^{-1}$) < 5-OH-EPAT (247.7 ± 12.1 $nmol.cm^{-2}.h^{-1}$). In a follow up study 2 additional concentrations (1.5 and 7.0 mM) of 5-OH-MPAT and 5-OH-EPAT were investigated. Comparing the flux of 5-OH-MPAT and 5-OH-EPAT after 9h of iontophoresis at 1.5 (99.6 ± 15.9 vs 68.7 ± 22.0 $nmol.cm^{-2}.h^{-1}$), 3.9 mM (see above) and 7.0 mM (404.9 ± 72.9 vs 354.2 ± 78.1 $nmol.cm^{-2}.h^{-1}$) showed no significant difference (2-way ANOVA; $p>0.05$) (Figure 3C). A similar trend was seen for iontophoretic transport studies across DHS: 8-OH-DPAC (168.2 ± 13.2 $nmol.cm^{-2}.h^{-1}$) < 5,6-di-OH-DPAT (175.2 ± 25.9 $nmol.cm^{-2}.h^{-1}$) < 5-OH-DPAT (193.0 ± 19.9 $nmol.cm^{-2}.h^{-1}$) < 5-OH-EPAT (199.8 ± 8.0 $nmol.cm^{-2}.h^{-1}$) < 5-OH-MPAT (241.8 ± 11.2 $nmol.cm^{-2}.h^{-1}$). A significant difference could be observed between the fluxes of the different compounds (1-way ANOVA; $p<0.05$).

3.4.2 Electroosmotic contribution across human stratum corneum

Acetaminophen (15 mM) was added to the donor solution to investigate the electroosmotic flow across HSC during iontophoretic transport. The resulting electroosmotic contribution, calculated using Equation 3, expressed as % of the total flux, is depicted in Figure 4. A significantly higher electro-osmotic contribution was observed when 5,6-di-OH-DPAT (12.1 ± 3.4 %) was transported through HSC,

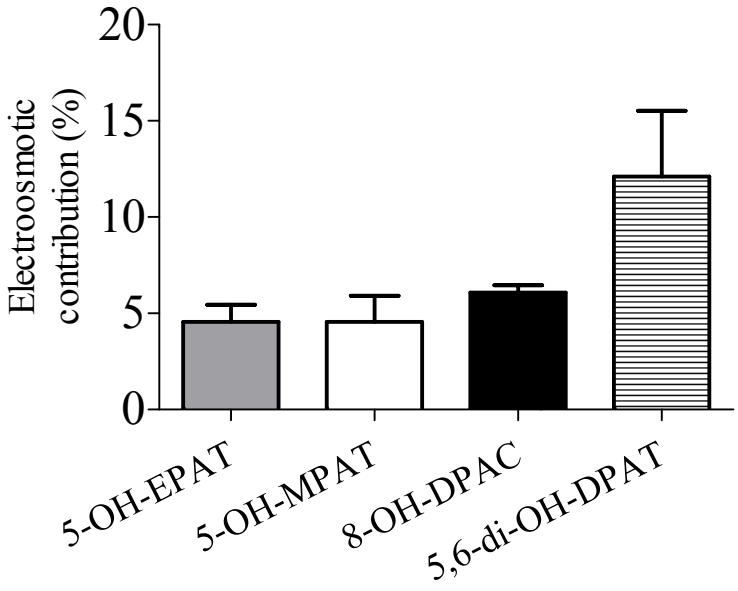

Figure 4: bar plot of the electroosmotic contribution during iontophoretic transport across human stratum corneum of different compounds. The donor concentration was 3.9 mM. Acetaminophen (15 mM) was co-transported to determine the electroosmotic flow during iontophoretic transport. The data are presented as mean ± SD (n=5-6).

compared to the other compounds 5-OH-EPAT (4.5 ± 0.9 %), 5-OH-MPAT (4.6 ± 1.4 %) and 8-OH-DPAC (6.1 ± 0.4 %) (1-way ANOVA, Bonferroni post test; $p<0.01$).

3.5 Model evaluation

The iontophoretic transport of the different compounds was fitted using the basic and extended model. The basic model assumes a constant input during iontophoresis with one skin release constant K_R. As an example the iontophoretic flux of 8-OH-DPAC (3.9 mM) across HSC is shown in Figure 5. The iontophoretic transport of 3.9 mM 8-OH-DPAC (open circle), together with the model predictions of the basic model (dashed line) clearly shows that the basic model does not fit to the experimental data. For this reason we employed the extended model with two release constants, K_{R1} and

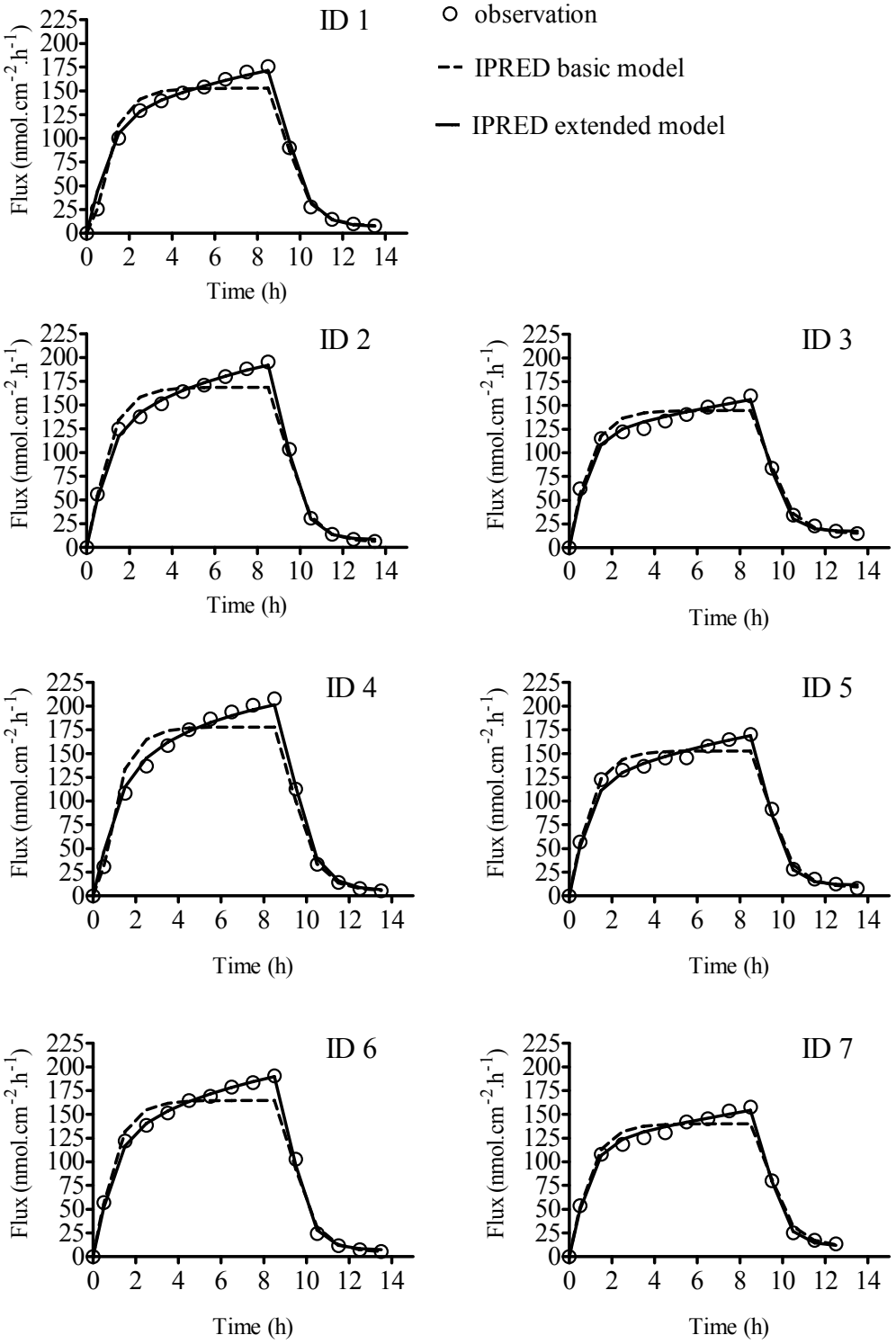

Figure 5: The individual iontophoretic flux (500 μA.cm^{-2}) vs time profiles of 8-OH-DPAC (3.9 mM) across human stratum corneum. The data are plotted as individual observations (open circle), together with the individual prediction (IPRED) based on the basic *in vitro* model (intermittent line) and on the extended *in vitro* model with two different release constants (solid line)

Table 3: The parameter estimates of data fitting the *in vitro* iontophoretic delivery (500 $\mu A.cm^{-2}$) across human stratum corneum (HSC) and dermatomed human skin (DHS) of the various 2-aminotetralins and chromanamine. The intrinsic driving force corrected for the surface area (I_0/S), the skin release constants (K_{R1} and K_{R2}), the passive driving force post iontophoresis corrected for the surface area (P_{PI}/S;Pass) and the lag time (t_L) are depicted. The donor concentration was 3.9 mM. Results are presented as population mean ± standard error of the estimate (n=4-7).

skin type	Compound		I_0/S		K_{R1} (slow)		K_{R2} (fast)		Pass		t_L	
			$nmol.cm^{-2}.h^{-1}$		h^{-1}		h^{-1}		$nmol.cm^{-2}.h^{-1}$		h	
		n	Mean	SE	Mean	SE	Mean	SE	Mean	SE	Mean	SE
HSC	5-OH-EPAT	6	176.56	9.33	0.06	0.02	1.43	0.13	3.17	0.58	n.d.	n.d
	5-OH-MPAT	5	178.13	6.36	0.02	0.02	1.63	0.09	3.33	0.23	n.d.	n.d
	5,6-di-OH-MPAT	5	133.28	5.11	n.d	n.d	1.38	0.23	n.d	n.d	0.08	0.13
	5,6-di-OH-DPAT	5	91.25	1.86	0.43	0.12	1.19	0.07	2.77	1.28	0.06	0.05
	8-OH-DPAC	7	113.91	2.55	0.09	0.01	1.41	0.04	8.82	1.72	0.14	0.05
	5-OH-DPAT[a]	6	119.69	8.67	0.25	0.15	1.39	0.14	4.47	0.74	0.06	0.07
	rotigotine.HCl[b]	6	45.31	0.42	0.32	0.10	0.96	0.06	20.30	0.39	n.d	n.d
DHS	5-OH-EPAT	6	99.22	2.25	1.27	0.69	0.46	0.04	0.02	n.d	0.27	0.01
	5-OH-MPAT	7	118.91	1.49	0.47	0.11	0.54	0.04	4.64	1.32	0.26	0.08
	5,6-di-OH-DPAT	6	116.25	2.66	0.08	0.02	0.63	0.02	10.10	1.12	0.21	0.05
	8-OH-DPAC	7	101.88	1.12	0.08	0.04	0.53	0.04	n.d	n.d	0.47	0.08
	5-OH-DPAT	4	95.16	1.43	0.73	0.33	0.56	0.06	5.15	2.99	0.22	0.03
	rotigotine.HCl[b]	6	35.31	3.33	0.03	0.02	0.28	0.04	22.70	1.62	n.d	n.d

[a,b]: data was adapted from literature[14, 40]
n.d: not determined because the parameter was constrained to 0

K_{R2}. The extended model describes more adequately the flux of the drug than the basic model (Figure 5, solid line). This graphical analysis was performed for all compounds across DHS and HSC. The majority of the individual fits showed an improvement when using the extended model. The two models were also evaluated statistically by comparison of the objective function of the models. Except for rotigotine.HCl across DHS and 5,6-di-OH-MPAT across HSC, in all cases the objective function decreased with a value larger than 3.84. This indicates that although an extra parameter (K_{R2}) was added to the model, a clear improvement in fitting the iontophoretic transport across HSC and DHS was obtained ($p<0.05$; Chi-square test). A model using two zero order mass input rates (I_0) or an additional release constant (K_{R3}) did not further improve data fitting. The estimated transport parameters, using the extended model with one zero order mass input rate and 2 release constants, can be found in Table 3.

4 Discussion

In this study the transdermal iontophoretic delivery of a series of 2-aminotetralins and 1 chromanamine (8-OH-DPAC) is presented. The systematic structural differences of these compounds allowed us to investigate the effect of molecular structure on the solubility and on iontophoretic delivery efficiency.

4.1 Solubility

The differences in structure highly affected the solubility of the various compounds. Compared to 5-OH-DPAT, approximately a 2-fold higher solubility was observed for 5-OH-EPAT and 5-OH-MPAT, indicating that decreasing the length of the alkyl side chain on the nitrogen group improves the solubility of the compound, most probably due to reduction in lipophilicity and an increase in chargeability of the nitrogen group. Furthermore for 8-OH-DPAC almost a 5-fold higher solubility was observed compared to 5-OH-DPAT. This demonstrates that replacement of the tetrahydronaphtalene moiety, present in the structure of 5-OH-DPAT, by a chroman moiety (as in 8-OH-DPAC), increases the solubility. In contrast, 5,6-di-OH-DPAT showed a reduced solubility, which can be explained by the formation of intermolecular hydrogen bridges, decreasing its water solubility.

4.2 Efficiency of iontophoretic transport

Small structural changes influence the transport efficiency of the different analogs significantly across HSC and DHS. Although steady state had not been reached yet after 9h of current application, already a clear difference can be observed at this time point. Despite the increase in hydrophilicity of 5,6-di-OH-MPAT and 5,6-di-OH-DPAT by introducing an extra oxygen on the phenylring, the iontophoretic flux reduced, compared to 5-OH-MPAT and 5-OH-DPAT. It has been reported that an increase in molecular volume results in a decrease in total iontophoretic flux, but in an increase in electroosmotic contribution [24, 43]. The significantly higher electroosmotic contribution for 5,6-di-OH-DPAT might be due to an increased molecular volume, caused by intermolecular hydrogen bonds, which would also account for the reduced iontophoretic flux. Decreasing the alkyl length of one side chain on the nitrogengroup from propyl (5-OH-DPAT) to ethyl (5-OH-EPAT) or further to a hydrogen (5-OH-MPAT) resulted in an increased efficiency of iontophoretic transport. This is in agreement with the observations by Del Terzo *et al.*, who obtained a similar result with ionized n-alkalanoic acids [29].

4.3 Transport pathways

In literature different iontophoretic transport routes are proposed: (i) the transport route across the appendageal structures, such as hair follicles and sweat glands, and (ii) the transport route via the intercellular route in the skin [44-47]. In agreement, fitting the iontophoretic flux using a model with two release constants also suggests the presence of at least 2 different transport routes across human skin during current application. In the initial time period of iontophoresis transport across the more permeable pores, possibly the appendages, with a faster release to the acceptor phase (described by K_{R2}) is the major contributor to the total iontophoretic flux. However, when the iontophoresis proceeds, the contribution of the second penetration route, suggested as the intercellular pathway, with a slower release (described by K_{R1}) increases. This results in an increase in the total iontophoretic flux (Figure 5). Modeling transport across HSC and DHS post iontophoresis revealed that the release from the skin was best described by K_{R2}. This suggests that the appendageal route post iontophoresis is still the predominant route. Similar observations by Turner and co-workers reported that the predominant transport route for the ionized calcein after iontophoresis pre-treatment was via the pores [47].

Comparing the skin release constant K_{R2} for HSC and DHS transport, it was observed that K_{R2} was smaller during transport across DHS. This can at least partly be attributed by the presence of hydrophilic regions and negative charged cell

membranes at pH 7.4 in both the epidermis and the upper part of the dermis, slowing down the partitioning of the compounds from the skin to the acceptor phase.

4.4 Physicochemical considerations for iontophoretic delivery

In literature several *in vitro* methods have been proposed as first screening methods for transdermal iontophoretic delivery. The molecular descriptors for iontophoresis in these methods were charge, molecular weight/volume and ionic/electrophoretic mobility [28, 33, 48-49].

As the electrophoretic mobility was reported as a good descriptor for the electromigrative flux (J_{EM}) [28, 33], in the present study, J_{EM} after 9h of iontophoresis was calculated using Equation 2. The passive flux was considered to be negligible. For the transport studies across HSC J_{EM} correlated linearly with the electrophoretic mobility (R^2=0.85) (Figure 6C).

Although capillary electrophoresis to estimate the J_{EM} at 9h is a good screening method for transdermal iontophoresis, this single end-point approach has some limitations. Firstly, this approach assumes that the end-point is representative for the entire iontophoretic flux, also before and after this point. However it does not account for the shape of the curve. Secondly, it is also important to understand the influence of the physicochemical properties on the different transport parameters, such as the zero order mass input and the release constants (Table 3). This information is important to make a realistic extrapolation towards *in vivo*. The iontophoretic mass transfer is driven by a potential gradient. This implies that besides the current density and the donor composition, which are kept constant in the transport studies, the zero order mass transfer is dependent on the electrophoretic properties of the molecule. It is observed that the zero order mass input, corrected for the surface area (I_0/S), is linearly correlated to the electrophoretic mobility (R^2=0.93) (Figure 6A). This also means that the steady state flux, calculated using Equation (8), can be predicted by the electrophoretic mobility. Previous studies demonstrated that the transport efficiency decreased with increasing molecular weight (Mw) [24-26]. For instance Lai and co-worker considered in the ionic mobility-pore model, that the logarithm of the permeability coefficient decreases linearly with increasing Mw [24]. If our interpretations are correct and K_{R2} describes the release during appendageal transport, it can be expected that the release from these pores into the acceptor phase is size dependent. Plotting the fast release constant K_{R2} against the Mw confirms this size dependency. The fast release constant K_{R2} is reduced linearly with increased Mw (Figure 6B; R^2=0.90).

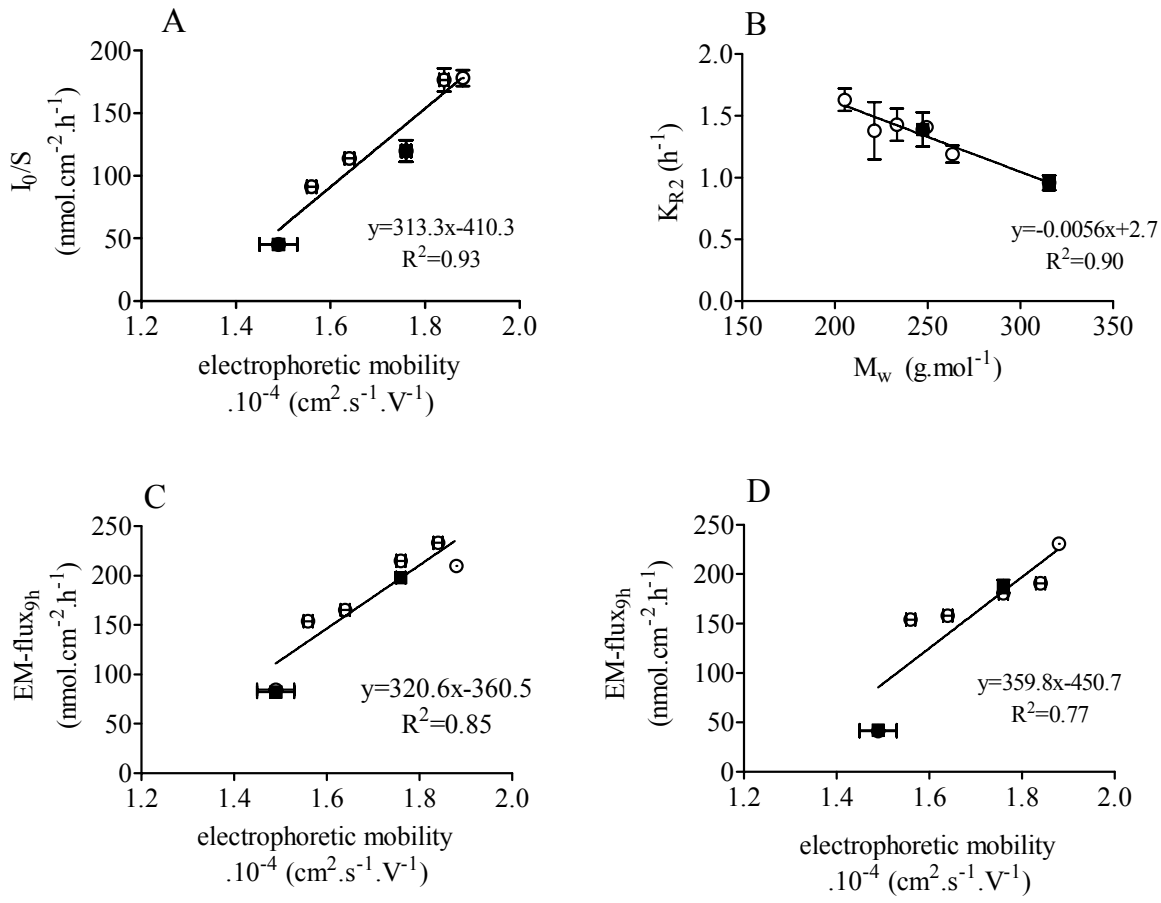

Figure 6: The relationships between the physicochemical properties of the compounds (open circle) and the transport parameters. The data of 5-OH-DPAT and rotigotine (closed square) were added to the graphs and included in the correlations. In all cases the donor concentration of the dopamine agonist was 3.9 mM. Data are presented as mean ± SD for the EM-flux and electrophoretic mobilty (n≥3). The parameter estimates (I_0 and K_{R2}) are presented as mean ± standard error of the estimate (n≥4). The regression analysis was performed with the mean point estimates. **A**: The linear correlation between the intrinsic driving force corrected for the surface area (I_0/S) vs the mean electrophoretic mobility. **B**: The linear correlation between the K_{R2} and the molecular weight. **C**: The electromigrative flux (EM-flux) at 9h across human stratum corneum is plotted against the mean electrophoretic mobility. **D**: The correlation between the flux at 9h across dermatomed human skin versus the mean electrophoretic mobility.

Although not fully understood yet, the lipophilicity of the molecules can be of importance for the transport efficiency and transport pathway. For instance Jadoul *et al*. showed that fentanyl, a relatively lipophilic molecule, was distributed across the whole HSC, while the more hydrophilic thyrotropin releasing hormone was mainly localized in the pores after iontophoresis [50]. In analogy, our observations show that the relative contribution of the two different transport pathways is dependent on the lipophilicity of the solute. For the more lipophilic compounds, rotigotine and 5-OH-DPAT, a relatively high K_{R1} value was observed, while for the more hydrophilic compounds K_{R1} remained small. For the most hydrophilic compound 5,6-di-OH-MPAT even a negligible value for K_{R1} was observed. An exception was made for 5,6-di-OH-DPAT, since other mechanisms play a role in its iontophoretic transport.

Due to the increased membrane complexity of DHS, the aforementioned relationships between the physicochemical properties (electrophoretic mobility, Mw, clogP) and the transport parameters (J_{EM}, I_0/S, K_{R2}, K_{R1}) were not so evident, contrasting the observations for transport across HSC. For instance across DHS, assuming that the relative electromigrative contribution is similar to that across HSC, the linear correlation between the J_{EM} and the electrophoretic mobility was not so clear (Figure 6D) (R^2=0.78). DHS includes HSC, the viable epidermis, and a part of the dermis, and therefore the complexity of the transport membrane augments. Further research is necessary to fully understand the underlying transport mechanism(s) involved in epidermal transport. A larger set of molecules, covering a broader range of electrophoretic mobilities presumably will increase the predictive value of capillary electrophoresis for the J_{EM} across DHS, as was observed for a series of dipeptides [28, 33]. These dipeptides were grouped in 3 clusters, where the correlation within the groups was far less than the overall correlation, including all 11 peptides. Nonetheless the electrophoretic mobility and the corresponding J_{EM} across DHS, observed for the dopamine agonists in the current paper were similar to the values obtained for the dipeptides at pH 7.4 [28, 33].

Next to identifying the physicochemical-transport parameter relationships, compartmental modeling can be very useful for extrapolation towards the *in vivo* situation. Assuming transport across HSC *in vitro* is representative for transport *in vivo* in humans, combining these transport parameters with pharmacokinetic parameters, applying non-linear mixed effect modeling, simulations can be made of the iontophoretic flux *in vivo*. Nugroho *et al*. demonstrated that for transdermal iontophoresis such an extrapolation from *in vitro* to *in vivo* is possible in rats, predicting the plasma concentration and even the pharmacodynamic effect [16].

In conclusion, this study shows that small structural changes affect the solubility, electrophoretic mobility, the iontophoretic delivery efficiency and the contribution of the transport route during iontophoresis. Increasing the hydrophilicity by addition of an extra OH-group on the phenyl ring (5,6-di-OH-MPAT and 5,6-di-OH-DPAT) did not result in an increase in solubility nor transport efficiency. On the other hand solubility and iontophoretic transport can benefit from reduction in the alkyl groups at the nitrogen. In addition the electrophoretic mobility and the Mw can be applied to estimate the zero order mass input I_0/S and K_{R2}, respectively. The clogP might be helpful in determination of the relative contribution of the different transport pathways by estimation of K_{R1}, although further research is required to define a clear relationship. With the estimated parameters, using the proposed compartmental model, it will be possible to simulate the iontophoretic flux profile across HSC *in vitro*. Simulations can be a helpful tool in designing future experiments, giving the opportunity to explore different flux profiles and different study designs.

Acknowledgements

This research was financially supported by a grant (LKG 6507) of the Dutch Technology Foundation STW, Utrecht, The Netherlands.

References

1. Sage, B.H., *Iontophoresis*, in *Percutaneous Penetration Enhancers*, E.W. Smith and H.I. Maibach, Editors. 1995, CRC Press Inc.: Boca Raton. p. 351-365.
2. Nutt, J.G., *Continuous dopaminergic stimulation: Is it the answer to the motor complications of Levodopa?* Mov Disord, 2007. **22**(1): p. 1-9.
3. Olanow, C.W., *The scientific basis for the current treatment of Parkinson's disease.* Annu Rev Med, 2004. **55**: p. 41-60.
4. Olanow, C.W., M.B. Stern, and K. Sethi, *The scientific and clinical basis for the treatment of Parkinson disease (2009).* Neurology, 2009. **72**(21 Suppl 4): p. S1-136.
5. van Laar, T., et al., *Stepwise intravenous infusion of apomorphine to determine the therapeutic window in patients with Parkinson's disease.* Clin Neuropharmacol, 1998. **21**(3): p. 152-8.
6. Tugwell, C., *Parkinson's disease in focus*. 1st ed. In focus. 2008, London: Pharmaceutical Press. 237.
7. van der Geest, R., M. Danhof, and H.E. Bodde, *Iontophoretic delivery of apomorphine. I: In vitro optimization and validation.* Pharm Res, 1997. **14**(12): p. 1798-803.
8. van der Geest, R., et al., *Iontophoretic delivery of apomorphine. II: An in vivo study in patients with Parkinson's disease.* Pharm Res, 1997. **14**(12): p. 1804-10.
9. Li, G.L., et al., *Transdermal iontophoretic delivery of apomorphine in patients improved by surfactant formulation pretreatment.* J Control Release, 2005. **101**(1-3): p. 199-208.
10. Li, G.L., et al., *Iontophoretic R-apomorphine delivery in combination with surfactant pretreatment: in vitro validation studies.* Int J Pharm, 2003. **266**(1-2): p. 61-8.
11. Luzardo-Alvarez, A., M.B. Delgado-Charro, and J. Blanco-Mendez, *Iontophoretic delivery of ropinirole hydrochloride: effect of current density and vehicle formulation.* Pharm Res, 2001. **18**(12): p. 1714-20.
12. Luzardo-Alvarez, A., M.B. Delgado-Charro, and J. Blanco-Mendez, *In vivo iontophoretic administration of ropinirole hydrochloride.* J Pharm Sci, 2003. **92**(12): p. 2441-8.
13. Nugroho, A.K., et al., *Transdermal iontophoresis of rotigotine: influence of concentration, temperature and current density in human skin in vitro.* J Control Release, 2004. **96**(1): p. 159-67.
14. Nugroho, A.K., et al., *Transdermal iontophoresis of rotigotine across human stratum corneum in vitro: influence of pH and NaCl concentration.* Pharm Res, 2004. **21**(5): p. 844-50.
15. Nugroho, A.K., et al., *Transdermal iontophoresis of the dopamine agonist 5-OH-DPAT in human skin in vitro.* J Control Release, 2005. **103**(2): p. 393-403.
16. Nugroho, A.K., et al., *Pharmacokinetics and pharmacodynamics analysis of transdermal iontophoresis of 5-OH-DPAT in rats: in vitro-in vivo correlation.* J Pharm Sci, 2006. **95**(7): p. 1570-85.
17. Beart, P.M., et al., *Radioreceptor binding reveals the potencies of N,N-disubstituted 2-aminotetralins as D2 dopamine agonists.* Naunyn Schmiedebergs Arch Pharmacol, 1987. **336**(5): p. 487-93.
18. Beaulieu, M., et al., *N,N-disubstituted 2-aminotetralins are potent D-2 dopamine receptor agonists.* Eur J Pharmacol, 1984. **105**(1-2): p. 15-21.
19. Hacksell, U., et al., *N-Alkylated 2-aminotetralins: central dopamine-receptor stimulating activity.* J Med Chem, 1979. **22**(12): p. 1469-75.
20. Horn, A.S., et al., *Synthesis and dopaminergic activity of a new oxygen isostere of the 2-aminotetralins: N,N-dipropyl-8-hydroxy-3-chromanamine.* Eur J Med Chem, 1988. **22**(4): p. 325-328.

21. Thorberg, S.O., et al., *Aminochromans: potent agonists at central dopamine and serotonin receptors.* Acta Pharm Suec, 1987. **24**(4): p. 169-82.
22. van Vliet, L.A., et al., *Affinity for dopamine D2, D3, and D4 receptors of 2-aminotetralins. Relevance of D2 agonist binding for determination of receptor subtype selectivity.* J Med Chem, 1996. **39**(21): p. 4233-7.
23. Vermue, N.A., et al., *Pharmacological profile of N,N dipropyl-8-hydroxy-3-chromanamine, an oxygen isostere of the dopamine agonist N,N dipropyl-5-hydroxy-2-aminotetralin with enhanced presynaptic selectivity.* Arch Int Pharmacodyn Ther, 1988. **293**: p. 37-56.
24. Lai, P.M. and M.S. Roberts, *An analysis of solute structure-human epidermal transport relationships in epidermal iontophoresis using the ionic mobility: pore model.* J Control Release, 1999. **58**(3): p. 323-33.
25. Roberts, M.S., P.M. Lai, and Y.G. Anissimov, *Epidermal iontophoresis: I. Development of the ionic-mobility pore model.* Pharm Res, 1998. **15**(10): p. 1569-1578.
26. Yoshida, N.H. and M.S. Roberts, *Solute molecular size and transdermal iontophoresis across excised human skin* Journal of controlled release, 1993. **25**(3): p. 177-195.
27. Abla, N., et al., *Effect of charge and molecular weight on transdermal peptide delivery by iontophoresis.* Pharm Res, 2005. **22**(12): p. 2069-78.
28. Abla, N., et al., *Capillary zone electrophoresis for the estimation of transdermal iontophoretic mobility.* J Pharm Sci, 2005. **94**(12): p. 2667-75.
29. Del Terzo, S., C.R. Behl, and R.A. Nash, *Iontophoretic transport of a homologous series of ionized and nonionized model compounds: influence of hydrophobicity and mechanistic interpretation.* Pharm Res, 1989. **6**(1): p. 85-90.
30. Schuetz, Y.B., et al., *Structure-permeation relationships for the non-invasive transdermal delivery of cationic peptides by iontophoresis.* Eur J Pharm Sci, 2006. **29**(1): p. 53-9.
31. Nugroho, A.K., et al., *Compartmental modeling of transdermal iontophoretic transport: I. In vitro model derivation and application.* Pharm Res, 2004. **21**(11): p. 1974-84.
32. Nugroho, A.K., et al., *Compartmental modeling of transdermal iontophoretic transport II: in vivo model derivation and application.* Pharm Res, 2005. **22**(3): p. 335-46.
33. Henchoz, Y., et al., *A fast screening strategy for characterizing peptide delivery by transdermal iontophoresis.* J Control Release, 2009.
34. Poole, S.K., et al., *Determination of acid dissociation constants by capillary electrophoresis.* J Chromatogr A, 2004. **1037**(1-2): p. 445-54.
35. Wan, H., et al., *Rapid screening of pKa values of pharmaceuticals by pressure-assisted capillary electrophoresis combined with short-end injection.* J Chromatogr A, 2002. **979**(1-2): p. 369-77.
36. Holford, N., *The Visual Predictive Check-Superiority to Standard Diagnostic (Rorschach) Plots.* PAGE 14, Abstr 738 [www.page-meeting.org/?abstract=738], 2005.
37. Tetko, I.V. and P. Bruneau, *Application of ALOGPS to predict 1-octanol/water distribution coefficients, logP, and logD, of AstraZeneca in-house database.* J Pharm Sci, 2004. **93**(12): p. 3103-10.
38. Tetko, I.V., et al., *Virtual computational chemistry laboratory--design and description.* J Comput Aided Mol Des, 2005. **19**(6): p. 453-63.
39. VCCLAB. *Virtual Computational Chemistry Laboratory,* http://www.vcclab.org. 2005.
40. Ackaert, O.W., et al., *Mechanistic studies of the transdermal iontophoretic delivery of 5-OH-DPAT in vitro.* J Pharm Sci, 2010. **99**(1): p. 275-85.
41. Cheng, H.Y., Strope, E., Adams, R.N. , *Electrochemical studies of the oxidation pathways of apomorphine.* Anal Chem, 1979. **51**(13): p. 2243-2246.
42. Afkhami, A., Nematollahi, D. ,Khalafi, L. , Rafiee, M., *Kinetic study of the oxidation of some catecholamines by digital simulation of cyclic voltammograms.* Int J Chem Kinet, 2005. **37**(1): p. 17-24.

43. Peck, K.D., et al., *Quantitative description of the effect of molecular size upon electroosmotic flux enhancement during iontophoresis for a synthetic membrane and human epidermal membrane.* J Pharm Sci, 1996. **85**(7): p. 781-8.
44. Alvarez-Roman, R., et al., *Visualization of skin penetration using confocal laser scanning microscopy.* Eur J Pharm Biopharm, 2004. **58**(2): p. 301-316.
45. Barry, W., ed. *Dermatological formulations. Percutaneous Absorption.* . 1983: New York: Marcel Dekker.
46. Cullander, C., *What are the pathways of iontophoretic current flow through mammalian skin?* Advanced Drug Delivey Reviews, 1992. **9**: p. 119-135.
47. Turner, N. and R.H. Guy, *Iontophoretic transport pathways: dependence on penetration physcicochemical properties.* J Pharm Sci, 1997. **86**(12): p. 1385-1389.
48. Mudry, B., et al., *Quantitative structure-permeation relationship for iontophoretic transport across the skin.* J Control Release, 2007. **122**(2): p. 165-72.
49. Yoshida, N.H. and M.S. Roberts, *Prediction of cathodal iontophoretic transport of various anions across excised skin from different vehicles using conductivity measurements.* J Pharm Pharmacol, 1995. **47**(11): p. 883-90.
50. Jadoul, A., et al., *Quantification and localization of fentanyl and trh delivered by iontophoresis in the skin* International Journal of Pharmaceutics, 1995. **120**(2): p. 221-228.